

Exotic Reaction Dynamics in the Gas-Phase Preparation of Anthracene (C₁₄H₁₀) via Spiroaromatic Radical Transients in the Indenyl–Cyclopentadienyl Radical–Radical Reaction

Chao He, Ralf I. Kaiser,* Wenchao Lu, Musahid Ahmed,* Yahaira Reyes, Stanislaw F. Wnuk, and Alexander M. Mebel*



Cite This: *J. Am. Chem. Soc.* 2023, 145, 3084–3091



Read Online

ACCESS |



Metrics & More

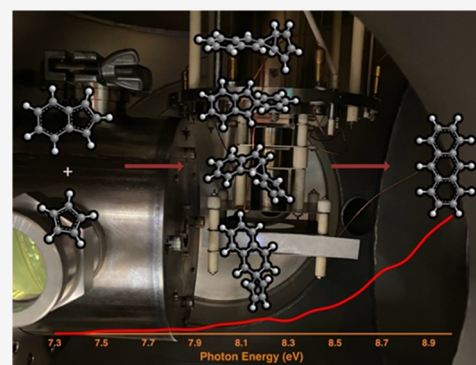


Article Recommendations



Supporting Information

ABSTRACT: The gas-phase reaction between the 1-indenyl (C₉H₇[•]) radical and the cyclopentadienyl (C₅H₅[•]) radical has been investigated for the first time using synchrotron-based mass spectrometry coupled with a pyrolytic reactor. Soft photoionization with tunable vacuum ultraviolet photons afforded for the isomer-selective identification of the production of phenanthrene, anthracene, and benzofulvalene (C₁₄H₁₀). The classical theory prevalent in the literature proposing that radicals combine only at their specific radical centers is challenged by our discovery of an unusual reaction pathway that involves a barrierless combination of a resonantly stabilized hydrocarbon radical with an aromatic radical at the carbon atom adjacent to the traditional C1 radical center; this unconventional addition is followed by substantial isomerization into phenanthrene and anthracene via a category of exotic spiroaromatic intermediates. This result leads to a deeper understanding of the evolution of the cosmic carbon budget and provides new methodologies for the bottom-up synthesis of unique spiroaromatics that may be relevant for the synthesis of more complex aromatic carbon skeletons in deep space.



INTRODUCTION

Since the first isolation of 9,9'-spirobifluorene (C₂₅H₁₆) by Clarkson and Gomberg in 1930,¹ aromatic spiro hydrocarbons—hydrocarbons carrying one atom common to two rings of orthogonally rigid structures (Scheme 1)—have attracted extensive attention from the organic preparative chemistry, physical organic chemistry, medicinal, and material science communities for use as semiconductors² and fluorescence dyes.³ This significance is based on the development of spirane-centered optoelectronic devices such as organic light-emitting diodes (OLEDs) with the spiro compound distinctively separating the hole and the electron; this spirane motif is central in minimizing the singlet–triplet energy splitting⁴ upon charge transfer considering the intramolecular donor–acceptor moiety augmented by spiro conjugation⁵ and spiro aromaticity.⁶ Although the spiro center formally interrupts the continuous conjugation and overlap of the spiro-fused π systems, essential properties linked with aromaticity like thermodynamical stability, aromatic ring currents, and nuclear shifts are still monitored for ladderized spirobifluorenes and indeno-spirobifluorenes.^{7,8} The chirality of aromatic spiranes not only enables essential bactericidal, fungicidal, anticancer, and herbicidal properties⁹ but also reveals circularly polarized luminescence such as for 10,10'-spirobi(indeno[1,2-*b*][1]benzothiophene) derivatives.^{10,11}

From the fundamental viewpoints of electronic structure theory and chemical bonding, spiro motif in polycyclic aromatic hydrocarbons (PAHs)—molecules carrying fused benzene rings—have been advocated as vital reaction intermediates in molecular mass growth processes leading via nanotubes¹² and fullerenes (C₆₀, C₇₀)¹³ to carbonaceous nanostructures (grains, soot) in high-temperature combustion systems and circumstellar envelopes of carbon stars (IRC + 10216) along with planetary nebulae as their descendants (TC 1).^{14,15} However, although aromatic structures have been discussed as possible carriers of the diffuse interstellar bands (DIBs)¹⁶ and of unidentified infrared emissions (UIRs)¹⁷ with PAH-like motif accounting for up to 30% of the cosmic carbon budget,¹⁸ the fundamental processes, which initiate and direct the formation of spirane-centered aromatics, have been inconclusive on the molecular level. Although proposed by Melius^{19–21} and suggested for the self-reaction of cyclopentadienyl radicals,^{22–25} not a single experiment has

Received: November 12, 2022

Published: January 26, 2023



Scheme 1. Simplest Spirane Spiro[2.2]penta-1,4-diene (C_5H_4 ; **1**) along with Spirobiindene ($C_{17}H_{12}$; **2**) and Spirobifluorene ($C_{25}H_{16}$; **3**)

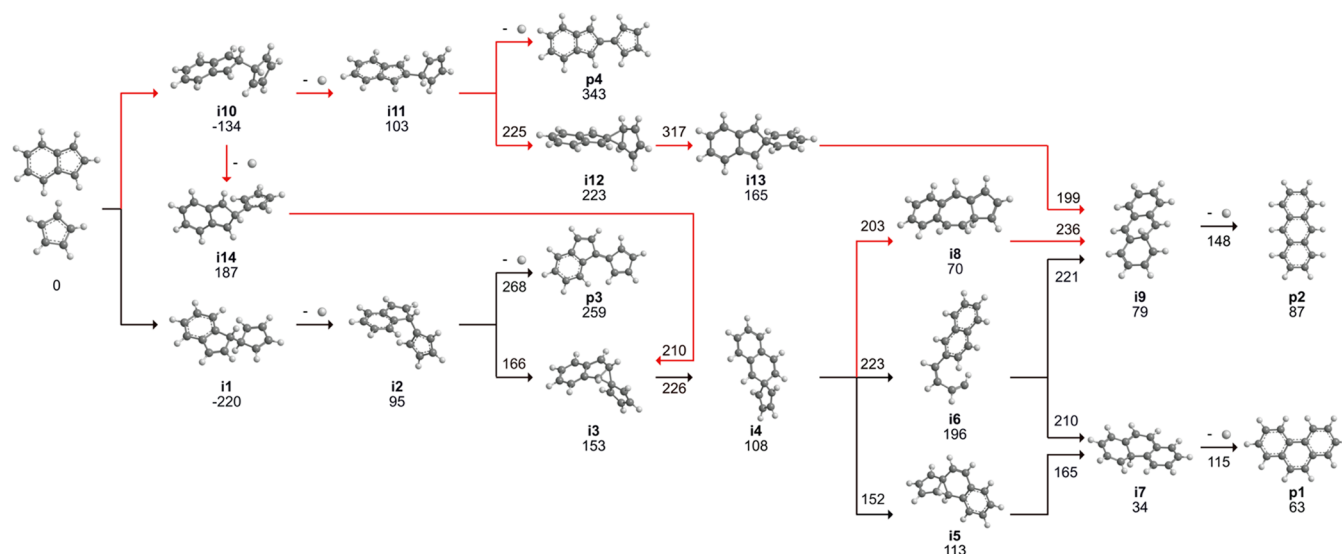
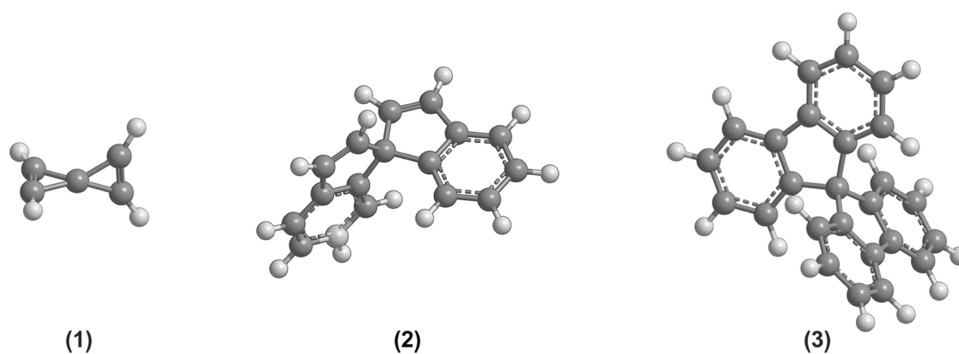


Figure 1. Dominant reaction pathways for the indenyl ($C_9H_7^\bullet$) plus cyclopentadienyl ($C_5H_5^\bullet$) reaction calculated at the G3(MP2,CC)/B2PLYPD3/6-311G(d,p) + ZPE(B2PLYPD3/6-311G(d,p)) level of theory. Traditional pathways extracted from ref 29 are colored in black, while the newly calculated channels are color-coded in red. The values on top of the arrows indicate energies of the transition states. All energies are given in kJ mol^{-1} with respect to the energy of the separated reactants. Atoms are colored in black (carbon) and gray (hydrogen).

documented the critical role of spirane-type aromatic intermediates in the gas-phase preparation of PAHs. This classifies spiranes as one of the most elusive classes of organic transient species in physical organic chemistry, computational chemistry, combustion sciences, and astrophysics.

Here, we report compelling evidence on the critical role of aromatic spiro transients in the gas-phase formation of phenanthrene ($C_{14}H_{10}$, **p1**), and anthracene ($C_{14}H_{10}$, **p2**), as the simplest, 14π -representative of helicenes and acenes, respectively, accessed through the reaction of the aromatic and resonantly stabilized 1-indenyl radical ($C_9H_7^\bullet$) with the cyclopentadienyl radical ($C_5H_5^\bullet$) in a high-temperature chemical microreactor (Figure 1). Validated through electronic structure calculations, discrete spiroaromatic hydrocarbon radical transients—1a',6a'-dihydro-5'H-spiro[cyclopentane-1,1'-cyclopropa[*a*]indene]-2,4-dienyl (**i3**), 4a'H-spiro[cyclopentane-1,2'-naphthalene]-2,4-dienyl (**i4**), 9b,9c-dihydro-3H-cyclopentadiene[2,3]cyclopropa[1,2-*a*]naphthalenyl (**i5**), spiro[bicyclo[3.1.0]hexane-6,2'-inden]-2-enyl (**i12**), and spiro[cyclohexane-1,2'-indene]-2,5-dienyl (**i13**) ($C_{14}H_{11}^\bullet$)—prepared through carbon–carbon coupling of the five-membered rings from the doublet radical reactants were revealed to be essential in the gas-phase preparation of

phenanthrene ($C_{14}H_{10}$, **p1**) and anthracene ($C_{14}H_{10}$, **p2**). Cemented through the isomer-selective identification of phenanthrene ($C_{14}H_{10}$, **p1**), anthracene ($C_{14}H_{10}$, **p2**), and benzofulvalene ($C_{14}H_{10}$, **p3**) in a molecular beam via fragment-free, soft photoionization by tunable synchrotron vacuum ultraviolet (VUV) light coupled with a reflectron time-of-flight mass spectrometer (Re-TOF-MS;^{26–28} Supporting Information), these findings afford persuasive testimony on a hitherto elusive class of aromatic, reactive intermediates involved in molecular mass growth processes of aromatics in our universe: spiroaromatics.

RESULTS

A representative mass spectrum recorded at a photon energy of 9.50 eV for the reaction of the 1-indenyl ($C_9H_7^\bullet$) radical with the cyclopentadienyl ($C_5H_5^\bullet$) radical at 1473 ± 10 K is displayed in Figure 2b. Control experiments of helium-seeded 1-bromoindene and anisole within the identical reactor were also carried out by keeping the silicon carbide tube at 298 K (Figure 2a). A comparison of both mass spectra provides compelling evidence that the signal at $m/z = 178$ ($C_{14}H_{10}^+$) and 180 ($C_{14}H_{12}^+$) originates from the 1-indenyl–cyclopentadienyl reaction at 1473 ± 10 K; this signal is clearly

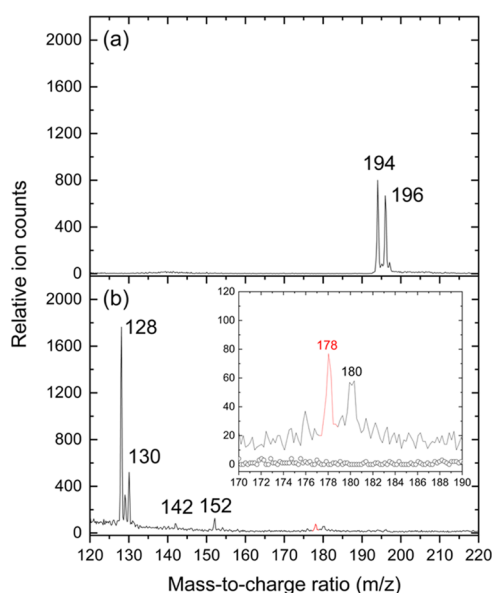


Figure 2. Photoionization mass spectra recorded at a photon energy of 9.50 eV for the indenyl ($C_9H_7^\bullet$) plus cyclopentadienyl ($C_5H_5^\bullet$) reaction at a temperature of 298 K (a) and 1473 ± 10 K (b). The insets highlight ion signals from $m/z = 170$ to 190 at 298 K (open circles) and 1473 ± 10 K (solid line), respectively.

absent in the control experiment. Accounting for the molecular weight of the reactants ($C_9H_7^\bullet$, 115 amu; $C_5H_5^\bullet$, 65 amu) and the products ($C_{14}H_{10}$, 178 amu; $C_{14}H_{12}$, 180 amu), the formation of molecules with the formula $C_{14}H_{12}$ can be linked to the radical-radical recombination of 1-indenyl with cyclopentadienyl; molecules with the molecular formula $C_{14}H_{10}$ can be formed from $C_{14}H_{12}$ through the loss of two hydrogen atoms. Further, ion counts are observable at $m/z = 128$ ($C_{10}H_8^+$), 129 ($^{13}CC_9H_8^+$), 130 ($C_{10}H_{10}^+$), 142 ($C_{11}H_{10}^+$), and 152 ($C_{12}H_8^+$; Figure S1). It should be highlighted that under identical microreactor conditions, the cyclopentadienyl ($C_5H_5^\bullet$) self-reaction was found not to lead to the formation of anthracene or phenanthrene.²⁶ Consequently, the analysis of the mass spectra of the present experiments alone reveals that the reaction of 1-indenyl ($C_9H_7^\bullet$) with the cyclopentadienyl ($C_5H_5^\bullet$) radical reveals vital molecular mass growth processes synthesizing hydrocarbon molecule(s) with the molecular formulae $C_{14}H_{10}$ and $C_{14}H_{12}$ in the gas phase.

A detailed analysis of the corresponding photoionization efficiency (PIE) curves, which report the intensity of the ions at $m/z = 178$ ($C_{14}H_{10}^+$) and 180 ($C_{14}H_{12}^+$) as a function of the photon energy from 7.30 to 9.0 eV, will allow for the identification of the structural isomers present at the relevant mass. The experimental PIE curve at $m/z = 178$ can be replicated by the sum of three $C_{14}H_{10}$ isomers: phenanthrene ($C_{14}H_{10}$, **p1**), anthracene ($C_{14}H_{10}$, **p2**), and benzofulvalene ($C_{14}H_{10}$, **p3**; Figure 3). The onset of the ion counts at 7.40 \pm

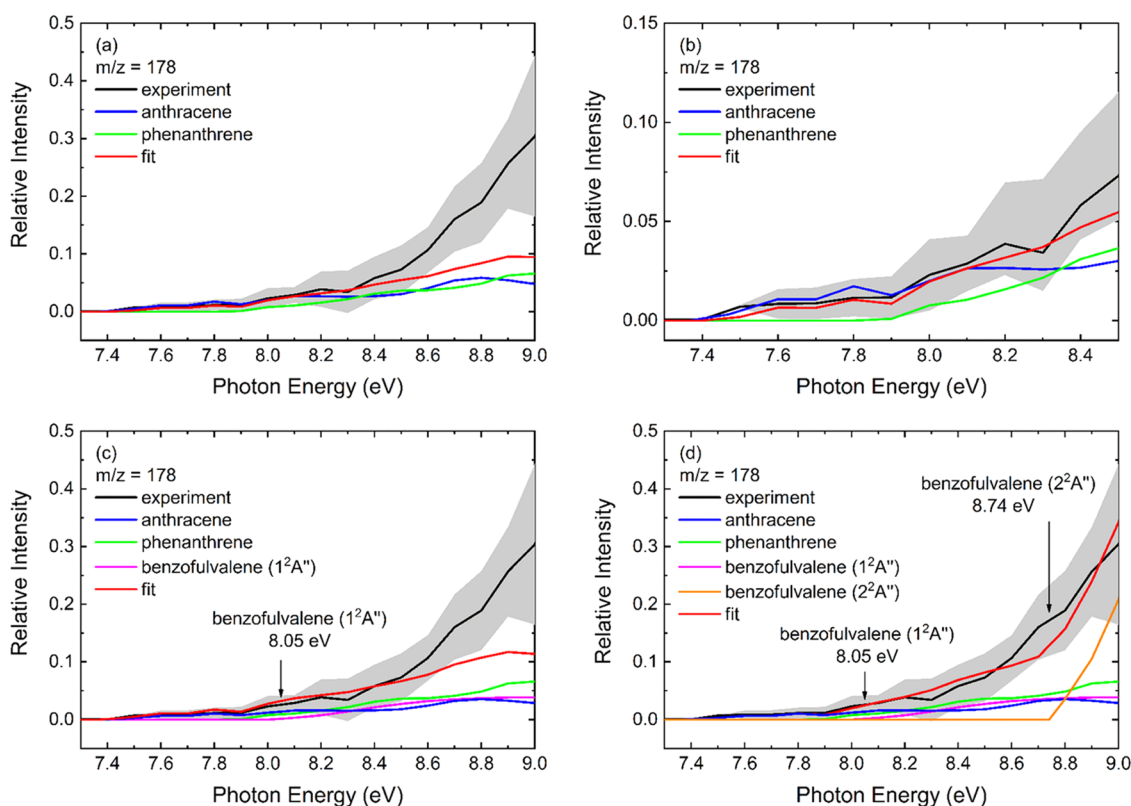


Figure 3. Photoionization efficiency (PIE) curves for products of interest formed in the reaction of indenyl ($C_9H_7^\bullet$) with cyclopentadienyl ($C_5H_5^\bullet$) at a reactor temperature of 1473 ± 10 K. (a) Fit (red) of the reference PIE curves of phenanthrene ($C_{14}H_{10}$, green) and anthracene ($C_{14}H_{10}$, blue) to the experimental $m/z = 178$ data (black) along with the zoomed range from 7.3 to 8.5 eV (b). (c) Fit (red) with the addition of the reference PIE curve of the ground electronic state of the benzofulvalene cation ($1^2A''$, IE = 8.05 ± 0.05 eV, magenta). (d) Fit (red) of the further addition of the reference PIE curve of the first excited state of the benzofulvalene cation ($2^2A''$, IE = 8.74 ± 0.05 eV, orange). The error bars consist of two parts: $\pm 10\%$ based on the accuracy of the photodiode and a 1σ error of the PIE curve averaged over the individual scans.

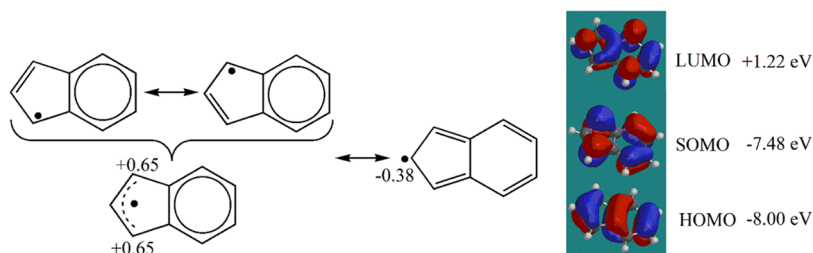


Figure 4. Resonance structures of the 1-indenyl radical (left) and its frontier molecular orbitals (right). The numbers show spin densities on the C1 (C3) and C2 atoms calculated at the B2PLYPD3/6-311G(d,p) level of theory.

0.05 eV correlates nicely with the NIST-evaluated adiabatic ionization energy (IE) of anthracene (**p2**) of 7.439 ± 0.006 eV (Figure 3a–d). Additional ion counts from phenanthrene (**p1**), which has an adiabatic ionization energy (IE) of 7.891 ± 0.001 eV,²⁷ are also critical; nevertheless, ion counts from phenanthrene ($C_{14}H_{10}$, **p1**) and anthracene ($C_{14}H_{10}$, **p2**) alone cannot replicate the experimental PIE curve. This discrepancy can be resolved by including a third isomer: benzofulvalene ($C_{14}H_{10}$, **p3**). The PIE curve of benzofulvalene ($C_{14}H_{10}$, **p3**) is unknown and hence has to be provided computationally (Supporting Information). The incorporation of ion counts from ionization of benzofulvalene ($C_{14}H_{10}$, **p3**) to the ground electronic state of the benzofulvalene cation ($1^2A''$, IE = 8.05 ± 0.05 eV) can replicate the experimental data up to 8.6 eV (Figure 3c); further inclusion of the first excited state of the benzofulvalene cation ($2^2A''$, IE = 8.74 ± 0.05 eV) provides an overall good match up to 9.0 eV of the experimental PIE curve (Figure 3d). Therefore, we may conclude that within our error limits, phenanthrene ($C_{14}H_{10}$, **p1**), anthracene ($C_{14}H_{10}$, **p2**), and benzofulvalene ($C_{14}H_{10}$, **p3**) contribute to the signal at $m/z = 178$ with the branching ratios of the ion counts of 19.3, 8.4, and 72.3%, respectively. Absolute photoionization cross sections of benzofulvalene (**p3**) are unknown and hence cannot be satisfactorily computed with accuracy levels of $\pm 10\%$. However, accounting for the photoionization cross sections of anthracene (**p2**) and phenanthrene (**p1**) of 16.7 ± 0.9 Mb and 17.2 ± 0.9 Mb, respectively, for 9.0 eV,³⁰ fractions of phenanthrene (**p1**) and anthracene (**p2**) of $63 \pm 5\%$ and $37 \pm 5\%$, respectively, can be extracted. The experimental PIE curve of benzofulvalene (**p3**) can be obtained by subtracting the contributions from anthracene (**p2**) and phenanthrene (**p1**) and hence is provided in Figure S2. Overall, the detailed analysis of the PIE curve at $m/z = 178$ reveals contributions from three isomers: phenanthrene ($C_{14}H_{10}$, **p1**), anthracene ($C_{14}H_{10}$, **p2**), and benzofulvalene ($C_{14}H_{10}$, **p3**). However, the quantification of anthracene ($C_{14}H_{10}$, **p2**) and phenanthrene ($C_{14}H_{10}$, **p1**) strongly contradicts previous electronic structure and kinetic calculations,²⁹ which deduced that the reaction of 1-indenyl with cyclopentadienyl should lead under our experimental conditions to a nearly exclusively benzofulvalene (**p3**) with upper limits of phenanthrene (**p1**) of 1%, but not to anthracene ($C_{14}H_{10}$, **p2**). The calculations also suggested that benzofulvalene (**p3**) can be efficiently converted to phenanthrene ($C_{14}H_{10}$, **p1**) via a secondary reaction of hydrogen atom-assisted isomerization at high temperatures, with the computed relative yield of anthracene ($C_{14}H_{10}$, **p2**) being only 2% at most at 1500 K. These deviations suggest that an understanding of the 1-indenyl–cyclopentadienyl radical–radical reaction is in its infancy with key reaction pathways to, e.g., anthracene ($C_{14}H_{10}$, **p2**) lacking. These discrepancies call for a

systematic computational investigation of the 1-indenyl–cyclopentadienyl reaction beyond the traditional mechanisms, leading to phenanthrene (**p1**) and benzofulvalene (**p3**; Figure 1 and Table S1).

DISCUSSION

Reaction pathways of the 1-indenyl radical with the cyclopentadienyl radical are compiled in Figure 1.²⁹ Traditionally, recombination of both radical reactants with the radical centers located at the C1 carbon atoms leads to the 1-(cyclopenta-2,4-dien-1-yl)-1*H*-indene intermediate ($C_{14}H_{12}$, **i1**) via carbon–carbon single bond coupling. The atomic hydrogen loss to doublet radical intermediate **i2** ($C_{14}H_{12}$) is endoergic by 315 kJ mol⁻¹. This intermediate can undergo yet another hydrogen loss preparing benzofulvalene (**p3**) or undergoes ring closure to tetracyclic spirane intermediate **i3**, which then rearranges through ring opening to the tricyclic spirane structure **i4**. Eventually, this doublet radical undergoes ring contraction or ring opening, yielding **i5** and **i6**, respectively. Both intermediates may isomerize to **i7**, which undergoes unimolecular decomposition through hydrogen atoms accompanied by aromatization and formation of phenanthrene (**p1**). The classical radical–radical recombination mechanism at the radical centers at the C1 atoms is unlikely to lead to anthracene (**p2**) in an overall endoergic reaction (87 kJ mol⁻¹) because the **i4** → **i6** → **i9** → **p2** route features much higher energy barriers than **i4** → **i5** → **i7** → **p1**. A hitherto overlooked pathway involving the reaction sequence **i4** → **i8** → **i9** followed by hydrogen loss can access anthracene (**p2**) but is also not competitive compared to **i4** → **i5** → **i7** → **p1**. A statistical treatment²⁹ of these reaction pathways starting from 1-(cyclopenta-2,4-dien-1-yl)-1*H*-inden-1-yl ($C_{14}H_{11}$) and 1*H*-inden-1-yl-2,4-cyclopentadien-1-ylidene (**i2**) predicts branching ratios of benzofulvalene (**p3**) to phenanthrene (**p1**) of 99.5 to 0.5%, and 98.9 and 1.1%, respectively, with practically no anthracene (**p2**) formed. The incorporation of a hydrogen atom-assisted isomerization of benzofulvalene (**p3**) opens up the production of anthracene (**p2**), but only at a level of 2% compared to phenanthrene (**p1**; 98%).²⁹ Clearly, the predicted ratio of phenanthrene (**p1**) to anthracene (**p2**) of 49 ± 5 does not match the experimentally derived ratio of 1.7 ± 0.5 . Therefore, a key pathway to anthracene (**p2**) is still lacking.

The classical reaction pathway as outlined in the aforementioned paragraph proceeds via recombination of cyclopentadienyl with the radical site on the C1 (C3) atom of 1-indenyl ($C_9H_7^\bullet$). However, the electronic structure of 1-indenyl can be described in terms of resonance allylic structures with radical positions on C1 and C3 and a methylic structure with the radical position on C2 (Figure 4). The two resonance structures correspond to the 2A_2 and 2B_1 electronic

states in the cyclopentadienyl radical ($C_5H_5^\bullet$), which are nearly degenerate in energy for C_5H_5 .^{31–33} Although the singly occupied molecular orbital (SOMO) in indenyl does not involve a contribution from the p_z orbital of C2, the highest doubly occupied orbital (HOMO), which is only 0.52 eV lower in energy, shows a significant role of $p_z(C2)$ (Figure 4). The calculated spin density on C2, $-0.38 e$, is roughly a factor of 2 lower by the absolute value than the spin densities on C1 and C3, $+0.65 e$. Owing to the significant spin density on C2, a barrierless addition of C_5H_5 to this atom is also feasible, although this process is less exoergic by 134 kJ mol^{-1} than the addition to C1 (C3) exoergic by 220 kJ mol^{-1} . Thus, considering the resonance structures and the spin density distribution in the 1-indenyl radical, one can rationalize a previously elusive barrierless radical–radical recombination of the cyclopentadienyl radical ($C_5H_5^\bullet$) with the C2 atom of 1-indenyl ($C_9H_7^\bullet$), leading to 2-(cyclopenta-2,4-dien-1-yl)-2H-indene (**i10**) via carbon–carbon bond coupling. Two successive hydrogen atom losses form 2-(cyclopenta-2,4-dien-1-ylidene)-2H-indene (**p4**) via 2H-indene-2,2-diyl-cyclopentadiene (**i11**). Note that, **p4** has an adiabatic IE of 7.02 eV, which is much lower than the experimental onset of the ion counts at $7.40 \pm 0.05 \text{ eV}$. Hence, the formation of **p4** can be eliminated as a predominant product. The key feature of 2H-indene-2,2-diyl-cyclopentadiene (**i11**) is its ability to isomerize to the spirane radical (**i12**) followed by ring opening to a second spirane radical (**i13**). Considering the inherent barriers along these pathways, the reaction sequence **i11** \rightarrow **i12** \rightarrow **i13** \rightarrow **i9** involving two distinct spirane structures is slightly energetically favorable compared to **i11** \rightarrow **p4** + H, by 26 kJ mol^{-1} considering the rate-controlling transition state for the **i12** \rightarrow **i13** step; this pathway terminates through atomic hydrogen loss accompanied aromatization and preparation of anthracene (**p2**). Note that **i10** can alternatively lose the hydrogen atom from the cyclopentadienyl moiety, leading to intermediate **i14**, which then easily isomerizes to **i3** thus merging onto the traditional reaction pathway toward phenanthrene. However, since **i14** resides 84 kJ mol^{-1} higher in energy than **i11**, the **i10** \rightarrow **i14** channel is unlikely to compete with **i10** \rightarrow **i11**. According to RRKM master equation calculations, at the experimental conditions, the unimolecular decomposition of **i11** to **p4** + H (98%) prevails over the multistep pathway to anthracene (**p2**) (2%), whereas the yield of phenanthrene (**p1**) is predicted to be negligible. Also, a fast hydrogen atom-assisted isomerization of **p4** predominantly leads to the formation of anthracene (**p2**), whereas the relative yield of phenanthrene (**p1**) in the **p4** + H reaction is predicted to be $\sim 1\%$. Overall, this reaction sequence can provide the “missing” source of anthracene (**p2**) as experimentally detected in the radical–radical reaction of 1-indenyl with cyclopentadienyl. The phenanthrene (**p1**)-to-anthracene (**p2**) branching ratio is thus mostly controlled by the initial branching in the entrance channel of the 1-indenyl-cyclopentadienyl radical–radical reaction between the addition of cyclopentadienyl to the C1 (C3) and C2 atoms in 1-indenyl. Accurate theoretical evaluation of the branching ratio for the two barrierless recombination channels is a complex dynamics problem, which can be in principle solved, e.g., through variable reaction coordinate transition state theory (VRC-TST) calculations. However, such calculations are extremely time-consuming and are beyond the scope of the present work. Based on the experimentally measured phenanthrene (**p1**)-to-anthracene (**p2**) branching ratio, the branching between

cyclopentadienyl radical addition to C1 (C3) and C2 should be approximately 2:1.

CONCLUSIONS

To conclude, our combined experimental and computational investigation of the reaction of the aromatic, resonantly stabilized 1-indenyl radical ($C_9H_7^\bullet$) with the cyclopentadienyl radical ($C_5H_5^\bullet$) reveals exotic reaction dynamics to an aromatic molecule—anthracene ($C_{14}H_{10}$)—which strongly contradicts an exclusive reaction mechanism of two radicals initiated by their recombination at the C1 radical centers. The unexpected reaction route engages a barrierless recombination of a doublet radical with an aromatic, resonantly stabilized radical at the central, C2 carbon atom of the allyl motif followed by extensive isomerization through exotic spiroaromatic doublet radical transients (**i12**, **i13**), thus connecting three previously disjointed concepts on the formation of aromatic molecules in the gas phase: resonance stabilization, aromaticity, spiro compounds. The key in the elucidation of the previously unknown reaction pathways to PAHs as provided here for reactions between two radicals is the isomer-selective identification of structural isomers through soft photoionization exploiting tunable vacuum ultraviolet light—a task that cannot be accomplished through traditional electron impact ionization of hydrocarbons^{34–36} and merging the experimental results with sophisticated electronic structure calculations. The unconventional reaction dynamics revealed here represents a benchmark of the recombination of two radicals holding five-membered rings and provides a versatile concept for gas-phase molecular mass growth processes to aromatic molecules and even three-dimensional nanostructures. Expanding the complexity, the self-recombination of two 1-indenyl radicals ($C_9H_7^\bullet$) is therefore forecasted to synthesize an unprecedented variety of structural PAH isomers—tetracene, [4]helicene, [4]phenacene ($C_{18}H_{12}$)—as simplest representatives of acenes, helicenes, and phenacenes, thus fundamentally contradicting traditional textbook knowledge of two radicals solely recombining at their unique radical centers and opening up novel pathways and a unified concept to molecular mass growth processes of aromatic structures in deep space through recombination of two radical species.

MATERIALS AND METHODS

Experimental Methods. The experiments were performed at the Chemical Dynamics Beamline (9.0.2.) of the Advanced Light Source (ALS) using a high-temperature chemical reactor consisting of a resistively heated silicon carbide (SiC) tube of 20 mm heating length and 1 mm inner diameter.³⁷ This device was located inside the source chamber of a molecular beam setup, which was equipped with a Wiley–McLaren reflectron time-of-flight mass spectrometer (RETOF-MS).³⁸ The indenyl radical ($C_9H_7^\bullet$) was prepared in situ by pyrolysis of the 1-bromoindene (C_9H_7Br) precursor synthesized in house using the procedure reported in previous work,³⁹ whereas a continuous beam of the cyclopentadienyl radical ($C_5H_5^\bullet$) was prepared in situ through the pyrolysis of anisole ($CH_3OC_6H_5$; Sigma-Aldrich).²⁶ The reactants were seeded in helium carrier gas at total pressures of $150 \pm 10 \text{ torr}$ at the reactor inlet through a 0.2 mm nozzle. The temperature of the SiC tube was determined using a Type-C thermocouple to be $1473 \pm 10 \text{ K}$. The precursor anisole ($CH_3OC_6H_5$; Sigma-Aldrich) was kept in a bubbler, whereas the 1-bromoindene (C_9H_7Br) precursor was stored in a Swagelok particulate filter. Both precursors were located outside the chamber and were maintained at room temperature of $298 \pm 3 \text{ K}$. At 1473 K, each precursor dissociated to the corresponding radical in situ as demonstrated previously^{26,37,40} followed by the reaction of the

indenyl ($C_9H_7^*$) and cyclopentadienyl ($C_5H_5^*$) radicals. The products formed in the reactor passed through a 2 mm skimmer located 10 mm downstream of the reactor and entered the main chamber, which houses the Re-TOF-MS. The neutral products within the supersonic molecular beam were then photoionized in the extraction region of the mass spectrometer by utilizing quasi-continuous tunable synchrotron vacuum ultraviolet (VUV) light. VUV single photon ionization represents essentially a fragment-free ionization technique and is accepted as a soft ionization method compared to the harsher conditions of electron impact ionization with the latter leading to excessive fragmentation of the parent ion.⁴¹ The ions formed via soft photoionization were extracted and ultimately detected by a microchannel plate detector through an ion lens. Under our experimental conditions, modeling suggested that the residence time in the reactor tube was few tens of microseconds.^{42,43} Photoionization efficiency (PIE) curves, which report ion counts as a function of photon energy with a step interval of 0.05 eV at a well-defined mass-to-charge ratio (m/z), were produced by integrating the signal recorded at the specific m/z for the species of interest. Due to the weak signal in these experiments, extended data accumulation times of up to 15 min per step had to be accounted for, and each step was repeated three times. No unexpected or unusually high safety hazards were encountered during the course of this study.

Computational Methods. The additional channels in the $C_9H_7 + C_5H_5$ reaction, which were not considered in the previous publication,²⁹ were explored here via doubly hybrid density functional theory (DFT) B2PLYPD3^{44–46}/6-311G(d,p) geometry optimization of the pertinent minima and transition states. Vibrational frequencies and zero-point vibrational energy (ZPE) corrections were computed at the same level of theory, and the optimized stationary structures were characterized as local minima or transition states on the PES based on the number of imaginary frequencies. Single-point energies were then refined within the G3(MP2,CC) model chemistry scheme.^{47–49} The B2PLYPD3 and G3(MP2,CC) calculations in the present study were performed using the Gaussian 16⁵⁰ and Molpro 2021⁵¹ quantum chemistry software packages. Adiabatic ionization energies of benzofulvalene isomers **p3** and **p4** were computed using the G3(MP2,CC)//B2PLYPD3/6-311G(d,p) method with ZPE corrections with the expected accuracy of ± 0.05 eV. Ionization Franck–Condon factors at 0 K needed to generate a theoretical photoionization efficiency (PIE) curve for **p3** were calculated using B2PLYPD3/6-311G(d,p)-optimized geometries and corresponding vibrational frequencies of the neutral and cationic species using the methodology implemented by Barone and co-workers.⁵² Electronic excitation energies of the benzofulvalene cation **p3**⁺ were estimated within the time-dependent (TD)-DFT method⁵³ with the ω B97XD functional⁵⁴ and the cc-pVTZ basis set.⁵⁵

Temperature- and pressure-dependent phenomenological rate constants for the decomposition of $C_{14}H_{11}$ radicals produced by H losses from the initial C_9H_7 - C_5H_5 complexes were computed using the one-dimensional Rice–Ramsperger–Kassel–Marcus master equation (RRKM-ME) approach⁵⁶ employing the MESS software package.⁵⁷ Details of the calculations were described in the previous work.²⁹ Here, we used the same MESS input file augmented with the additional intermediates, transition states, and product **p4**, which were included in the new kinetic scheme.

■ ASSOCIATED CONTENT

Data Availability Statement

All data needed to evaluate the conclusions in the paper are present in the paper and the [Supporting Information](#). Additional data are available from authors upon request.

SI Supporting Information

The Supporting Information is available free of charge at <https://pubs.acs.org/doi/10.1021/jacs.2c12045>.

Additional discussion of PIE Curves (Figures S1 and S2) and optimized Cartesian coordinates (Å) and vibrational frequencies (cm^{-1}) for the newly calculated pathways

involved in the indenyl ($C_9H_7^*$) plus cyclopentadienyl ($c-C_5H_5^*$) reaction (Table S1) ([PDF](#))

■ AUTHOR INFORMATION

Corresponding Authors

Ralf I. Kaiser – Department of Chemistry, University of Hawai'i at Manoa, Honolulu, Hawaii 96822, United States; orcid.org/0000-0002-7233-7206; Email: ralfk@hawaii.edu

Musahid Ahmed – Chemical Sciences Division, Lawrence Berkeley National Laboratory, Berkeley, California 94720, United States; orcid.org/0000-0003-1216-673X; Email: mahmed@lbl.gov

Alexander M. Mebel – Department of Chemistry and Biochemistry, Florida International University, Miami, Florida 33199, United States; orcid.org/0000-0002-7233-3133; Email: mebela@fiu.edu

Authors

Chao He – Department of Chemistry, University of Hawai'i at Manoa, Honolulu, Hawaii 96822, United States

Wenchao Lu – Chemical Sciences Division, Lawrence Berkeley National Laboratory, Berkeley, California 94720, United States; Present Address: CSIRO, Environment, Waite Campus, Urrbrae, South Australia 5064, Australia; orcid.org/0000-0002-3798-5128

Yahaira Reyes – Department of Chemistry and Biochemistry, Florida International University, Miami, Florida 33199, United States

Stanislaw F. Wnuk – Department of Chemistry and Biochemistry, Florida International University, Miami, Florida 33199, United States; orcid.org/0000-0002-3111-3919

Complete contact information is available at:

<https://pubs.acs.org/doi/10.1021/jacs.2c12045>

Notes

The authors declare no competing financial interest.

■ ACKNOWLEDGMENTS

This work was supported by the US Department of Energy, Basic Energy Sciences DE-FG02-03ER15411 (experimental studies) and DE-FG02-04ER15570 (computational studies) to the University of Hawaii (UH) and Florida International University (FIU), respectively. W.L. and M.A. were supported by the Director, Office of Science, Office of Basic Energy Sciences, of the U.S. Department of Energy under Contract No. DE-AC02-05CH11231, through the Gas Phase Chemical Physics program of the Chemical Sciences Division. The Advanced Light Source at Berkeley is also supported under Contract No. DE-AC02-05CH11231.

■ REFERENCES

- (1) Clarkson, R. G.; Gomberg, M. Spirans with Four Aromatic Radicals on the Spiro Carbon Atom¹. *J. Am. Chem. Soc.* **1930**, *52*, 2881–2891.
- (2) Saragi, T. P. I.; Spehr, T.; Siebert, A.; Fuhrmann-Lieker, T.; Salbeck, J. Spiro Compounds for Organic Optoelectronics. *Chem. Rev.* **2007**, *107*, 1011–1065.
- (3) Feng, J.; Fu, L.; Geng, H.; Jiang, W.; Wang, Z. Designing a Near-Infrared Circularly Polarized Luminescent Dye by Dissymmetric Spiro-Fusion. *Chem. Commun.* **2020**, *56*, 912–915.

- (4) Qu, Y.-K.; Zheng, Q.; Fan, J.; Liao, L.-S.; Jiang, Z.-Q. Spiro Compounds for Organic Light-Emitting Diodes. *Acc. Mater. Res.* **2021**, *2*, 1261–1271.
- (5) Milián-Medina, B.; Gierschner, J. Computational Design of Low Singlet–Triplet Gap All-Organic Molecules for OLED Application. *Org. Electron.* **2012**, *13*, 985–991.
- (6) Boivin, J.; Yousfi, M.; Zard, S. Z. Spirolactams by a Novel Ipso-Radical Cyclisation and Loss of Aromaticity. *Tetrahedron Lett.* **1997**, *38*, 5985–5988.
- (7) Meazza, M. *Spiro Compounds: A Brief History*. 2022, pp 1–8.
- (8) Liu, S.; Xia, D.; Baumgarten, M. Rigidly Fused Spiro-Conjugated π -Systems. *ChemPlusChem* **2021**, *86*, 36–48.
- (9) Chakraborty, K.; Antony, T. First Report of Spiro-Compounds from Marine Macroalga *Gracilaria Salicornia*: Prospective Natural Anti-Inflammatory Agents Attenuate 5-Lipoxygenase and Cyclooxygenase-2. *Nat. Prod. Res.* **2021**, *35*, 770–781.
- (10) Takase, K.; Noguchi, K.; Nakano, K. Circularly Polarized Luminescence from Chiral Spiro Molecules: Synthesis and Optical Properties of 10,10'-Spirobi[indeno[1,2-b][1]benzothiophene] Derivatives. *Org. Lett.* **2017**, *19*, 5082–5085.
- (11) Ding, A.; Meazza, M.; Guo, H.; Yang, J. W.; Rios, R. New Development in the Enantioselective Synthesis of Spiro Compounds. *Chem. Soc. Rev.* **2018**, *47*, 5946–5996.
- (12) Seyler, H.; Purushothaman, B.; Jones, D. J.; Holmes, A. B.; Wong, W. W. H. Hexa-Peri-Hexabenzocoronene in Organic Electronics. *Pure Appl. Chem.* **2012**, *84*, 1047–1067.
- (13) Hagen, S.; Bratcher, M. S.; Erickson, M. S.; Zimmermann, G.; Scott, L. T. Novel Syntheses of Three C₃₀H₁₂ Bowl-Shaped Polycyclic Aromatic Hydrocarbons. *Angew. Chem., Int. Ed.* **1997**, *36*, 406–408.
- (14) Zenobi, R.; Philippoz, J.-M.; Zare, R. N.; Buseck, P. R. Spatially Resolved Organic Analysis of the Allende Meteorite. *Science* **1989**, *246*, 1026–1029.
- (15) Yang, T.; Kaiser, R. I.; Troy, T. P.; Xu, B.; Kostko, O.; Ahmed, M.; Mebel, A. M.; Zagidullin, M. V.; Azyazov, V. N. HACA's Heritage: A Free-Radical Pathway to Phenanthrene in Circumstellar Envelopes of Asymptotic Giant Branch Stars. *Angew. Chem.* **2017**, *129*, 4586–4590.
- (16) Ricks, A. M.; Doublerly, G. E.; Duncan, M. A. The Infrared Spectrum of Protonated Naphthalene and Its Relevance for the Unidentified Infrared Bands. *Astrophys. J.* **2009**, *702*, 301.
- (17) Mori, T. I.; Sakon, I.; Onaka, T.; Kaneda, H.; Umehata, H.; Ohsawa, R. Diagnosis of PAH Properties and ISM Conditions Based on the Near-Infrared and Mid-Infrared UIR Bands. *Astron. Soc. Pac. Conf. Ser.* **2012**, *458*, 133–134.
- (18) Kalpana, M. S.; Babu, E. V. S. K.; Mani, D.; Tripathi, R. P.; Bhandari, N. Polycyclic Aromatic Hydrocarbons in the Mukundpura (CM2) Chondrite. *Planet. Space Sci.* **2021**, *198*, No. 105177.
- (19) Melius, C. F.; Colvin, M. E.; Marinov, N. M.; Pit, W. J.; Senkan, S. M. In *Reaction Mechanisms in Aromatic Hydrocarbon Formation Involving the C₅H₅ Cyclopentadienyl Moiety*, Symposium (International) on Combustion; Elsevier, 1996; pp 685–692.
- (20) Marinov, N. M.; Pitz, W. J.; Westbrook, C. K.; Vincitore, A. M.; Castaldi, M. J.; Senkan, S. M.; Melius, C. F. Aromatic and Polycyclic Aromatic Hydrocarbon Formation in a Laminar Premixed n-Butane Flame. *Combust. Flame* **1998**, *114*, 192–213.
- (21) Castaldi, M. J.; Marinov, N. M.; Melius, C. F.; Huang, J.; Senkan, S. M.; Pit, W. J.; Westbrook, C. K. In *Experimental and Modeling Investigation of Aromatic and Polycyclic Aromatic Hydrocarbon Formation in a Premixed Ethylene Flame*, Symposium (International) on Combustion; Elsevier, 1996; pp 693–702.
- (22) Kislov, V. V.; Mebel, A. M. The Formation of Naphthalene, Azulene, and Fulvalene from Cyclic C₅ Species in Combustion: An Ab Initio/RRKM Study of 9-H-Fulvalenyl (C₅H₅–C₅H₄) Radical Rearrangements. *J. Phys. Chem. A* **2007**, *111*, 9532–9543.
- (23) Mebel, A. M.; Kislov, V. V. Can the C₅H₅ + C₅H₅ → C₁₀H₁₀ → C₁₀H₈ + H/C₁₀H₈ + H₂ Reaction Produce Naphthalene? An Ab Initio/RRKM Study. *J. Phys. Chem. A* **2009**, *113*, 9825–9833.
- (24) Cavallotti, C.; Polino, D. On the Kinetics of the C₅H₅ + C₅H₅ Reaction. *Proc. Combust. Inst.* **2013**, *34*, 557–564.
- (25) Long, A. E.; Merchant, S. S.; Vandeputte, A. G.; Carstensen, H.-H.; Vervust, A. J.; Marin, G. B.; Van Geem, K. M.; Green, W. H. Pressure Dependent Kinetic Analysis of Pathways to Naphthalene from Cyclopentadienyl Recombination. *Combust. Flame* **2018**, *187*, 247–256.
- (26) Kaiser, R. I.; Zhao, L.; Lu, W.; Ahmed, M.; Zagidullin, M. V.; Azyazov, V. N.; Mebel, A. M. Formation of Benzene and Naphthalene through Cyclopentadienyl-Mediated Radical–Radical Reactions. *J. Phys. Chem. Lett.* **2022**, *13*, 208–213.
- (27) Kaiser, R. I.; Zhao, L.; Lu, W.; Ahmed, M.; Krasnoukhov, V. S.; Azyazov, V. N.; Mebel, A. M. Unconventional Excited-State Dynamics in the Concerted Benzyl (C₇H₇) Radical Self-Reaction to Anthracene (C₁₄H₁₀). *Nat. Commun.* **2022**, *13*, No. 786.
- (28) Zhao, L.; Lu, W.; Ahmed, M.; Zagidullin, M. V.; Azyazov, V. N.; Morozov, A. N.; Mebel, A. M.; Kaiser, R. I. Gas-Phase Synthesis of Benzene via the Propargyl Radical Self-Reaction. *Sci. Adv.* **2021**, *7*, No. eabf0360.
- (29) Krasnoukhov, V. S.; Zagidullin, M. V.; Zavershinskiy, I. P.; Mebel, A. M. Formation of Phenanthrene via Recombination of Indenyl and Cyclopentadienyl Radicals: a Theoretical Study. *J. Phys. Chem. A* **2020**, *124*, 9933–9941.
- (30) Li, Y.; Yang, J.; Cheng, Z. Photonionization Cross Section Database (Version 2.0). National Synchrotron Radiation Laboratory: Hefei, China, 2017, <http://flame.nsrl.ustc.edu.cn/database/data.php> (accessed 12 Jan, 2023).
- (31) Kiefer, J. H.; Tranter, R. S.; Wang, H.; Wagner, A. F. Thermodynamic Functions for the Cyclopentadienyl Radical: The Effect of Jahn–Teller Distortion. *Int. J. Chem. Kinet.* **2001**, *33*, 834–845.
- (32) Harding, L. B.; Klippenstein, S. J.; Georgievskii, Y. On the Combination Reactions of Hydrogen Atoms with Resonance-Stabilized Hydrocarbon Radicals. *J. Phys. Chem. A* **2007**, *111*, 3789–3801.
- (33) Ghildina, A. R.; Oleinikov, A. D.; Azyazov, V. N.; Mebel, A. M. Reaction Mechanism, Rate Constants, and Product Yields for Unimolecular and H-Assisted Decomposition of 2,4-Cyclopentadienone and Oxidation of Cyclopentadienyl with Atomic Oxygen. *Combust. Flame* **2017**, *183*, 181–193.
- (34) He, C.; Fujioka, K.; Nikolayev, A. A.; Zhao, L.; Doddipatla, S.; Azyazov, V. N.; Mebel, A. M.; Sun, R.; Kaiser, R. I. A Chemical Dynamics Study of the Reaction of the Methylidyne Radical (CH, X²II) with Dimethylacetylene (CH₃CCCH₃, X¹A_{1g}). *Phys. Chem. Chem. Phys.* **2021**, *24*, 578–593.
- (35) Casavecchia, P. Chemical Reaction Dynamics with Molecular Beams. *Rep. Prog. Phys.* **2000**, *63*, 355.
- (36) Thomas, A. M.; Zhao, L.; He, C.; Galimova, G. R.; Mebel, A. M.; Kaiser, R. I. Directed Gas-Phase Synthesis of Trifulvene under Single-Collision Conditions. *Angew. Chem., Int. Ed.* **2019**, *58*, 15488–15495.
- (37) Zhao, L.; Kaiser, R. I.; Lu, W.; Xu, B.; Ahmed, M.; Morozov, A. N.; Mebel, A. M.; Howlader, A. H.; Wnuk, S. F. Molecular Mass Growth through Ring Expansion in Polycyclic Aromatic Hydrocarbons via Radical–Radical Reactions. *Nat. Commun.* **2019**, *10*, No. 3689.
- (38) Parker, D. S. N.; Kaiser, R. I.; Troy, T. P.; Ahmed, M. Hydrogen Abstraction/Acetylene Addition Revealed. *Angew. Chem. Int. Ed.* **2014**, *53*, 7740–7744.
- (39) Zhao, L.; Prendergast, M. B.; Kaiser, R. I.; Xu, B.; Lu, W.; Ablikim, U.; Ahmed, M.; Oleinikov, A. D.; Azyazov, V. N.; Mebel, A. M.; et al. Reactivity of the Indenyl Radical (C₉H₇) with Acetylene (C₂H₂) and Vinylacetylene (C₄H₄). *ChemPhysChem* **2019**, *20*, 1437–1447.
- (40) Zhao, L.; Kaiser, R. I.; Lu, W.; Kostko, O.; Ahmed, M.; Evseev, M. M.; Bashkirov, E. K.; Oleinikov, A. D.; Azyazov, V. N.; Mebel, A. M.; et al. Gas Phase Formation of Cyclopentanaphthalene (Benzindene) Isomers via Reactions of 5- and 6-Indenyl Radicals with Vinylacetylene. *Phys. Chem. Chem. Phys.* **2020**, *22*, 22493–22500.

(41) Qi, F. Combustion Chemistry Probed by Synchrotron VUV Photoionization Mass Spectrometry. *Proc. Combust. Inst.* **2013**, *34*, 33–63.

(42) Guan, Q.; Urness, K. N.; Ormond, T. K.; David, D. E.; Barney Ellison, G.; Daily, J. W. The Properties of a Micro-Reactor for the Study of the Unimolecular Decomposition of Large Molecules. *Int. Rev. Phys. Chem.* **2014**, *33*, 447–487.

(43) Žagidullin, M. V.; Kaiser, R. I.; Porfiriev, D. P.; Zavershinskiy, I. P.; Ahmed, M.; Azyazov, V. N.; Mebel, A. M. Functional Relationships between Kinetic, Flow, and Geometrical Parameters in a High-Temperature Chemical Microreactor. *J. Phys. Chem. A* **2018**, *122*, 8819–8827.

(44) Grimme, S. Semiempirical hybrid density functional with perturbative second-order correlation. *J. Chem. Phys.* **2006**, *124*, No. 034108.

(45) Goerigk, L.; Grimme, S. Efficient and accurate Double-Hybrid-Meta-GGA density functionals-evaluation with the extended GMTKN30 database for general main group thermochemistry, kinetics, and noncovalent interactions. *J. Chem. Theory Comput.* **2011**, *7*, 291–309.

(46) Grimme, S.; Ehrlich, S.; Goerigk, L. Effect of the damping function in dispersion corrected density functional theory. *J. Comput. Chem.* **2011**, *32*, 1456–1465.

(47) Baboul, A. G.; Curtiss, L. A.; Redfern, P. C.; Raghavachari, K. Gaussian-3 Theory using Density Functional Geometries and Zero-Point Energies. *J. Chem. Phys.* **1999**, *110*, 7650–7657.

(48) Curtiss, L. A.; Raghavachari, K.; Redfern, P. C.; Baboul, A. G.; Pople, J. A. Gaussian-3 Theory using Coupled Cluster Energies. *Chem. Phys. Lett.* **1999**, *314*, 101–107.

(49) Curtiss, L. A.; Raghavachari, K.; Redfern, P. C.; Rassolov, V.; Pople, J. A. Gaussian-3 (G3) Theory for Molecules Containing First and Second-Row Atoms. *J. Chem. Phys.* **1998**, *109*, 7764–7776.

(50) Frisch, M. J.; Trucks, G. W.; Schlegel, H. B.; Scuseria, G. E.; Robb, M. A.; Cheeseman, J. R.; Scalmani, G.; Barone, V.; Mennucci, B.; Petersson, G. A. et al. *Gaussian 16*, Revision C.1; Gaussian Inc.: Wallingford, CT, 2019; Vol. 200, p 28.

(51) Werner, H.-J.; Knowles, P. J.; Knizia, G.; Manby, F. R.; Schütz, M.; Celani, P.; GYörfy, W.; Kats, D.; Korona, T.; Lindh, R. et al. *MOLPRO, Version 2021.2, A Package of Ab Initio Programs*; University of Cardiff: Cardiff, UK, 2021. <http://www.molpro.net>.

(52) Barone, V.; Bloino, J.; Biczysko, M.; Santoro, F. Fully Integrated Approach to Compute Vibrationally Resolved Optical Spectra: from Small Molecules to Macromolecules. *J. Chem. Theory Comput.* **2009**, *5*, 540–554.

(53) Scalmani, G.; Frisch, M. J.; Mennucci, B.; Tomasi, J.; Cammi, R.; Barone, V. Geometries and Properties of Excited States in the Gas Phase and in Solution: Theory and Application of a Time-Dependent Density Functional Theory Polarizable Continuum Model. *J. Chem. Phys.* **2006**, *124*, No. 094107.

(54) Chai, J.-D.; Head-Gordon, M. Long-Range Corrected Hybrid Density Functionals with Damped Atom–Atom Dispersion Corrections. *Phys. Chem. Chem. Phys.* **2008**, *10*, 6615–6620.

(55) Dunning, T. H. Gaussian Basis Sets for Use in Correlated Molecular Calculations. I. the Atoms Boron through Neon and Hydrogen. *J. Chem. Phys.* **1989**, *90*, 1007–1023.

(56) Georgievskii, Y.; Miller, J. A.; Burke, M. P.; Klippenstein, S. J. Reformulation and Solution of the Master Equation for Multiple-well Chemical Reactions. *J. Phys. Chem. A* **2013**, *117*, 12146–12154.

(57) Georgievskii, Y.; Klippenstein, S. J. *Master Equation System Solver (MESS)*, 2015, <https://tcg.cse.anl.gov/papr/codes/mess.html>.

Recommended by ACS

Light-Controlled Lyotropic Liquid Crystallinity of Polyaspartates Exploited as Photo-Switchable Alignment Medium

Max Hirschmann, Christina M. Thiele, et al.

FEBRUARY 07, 2023

JOURNAL OF THE AMERICAN CHEMICAL SOCIETY

READ 

Isomer-Dependent Threshold Photoelectron Spectroscopy and Dissociative Photoionization Mechanism of Anisaldehyde

Xiangkun Wu, Andras Bodi, et al.

JANUARY 11, 2023

THE JOURNAL OF PHYSICAL CHEMISTRY A

READ 

Negative Photochromic 3-Phenylperylene-bridged Imidazole Dimer Offering Quantitative and Selective Bidirectional Photoisomerization with Visible and Near-In...

Natsuho Moriyama and Jiro Abe

FEBRUARY 07, 2023

JOURNAL OF THE AMERICAN CHEMICAL SOCIETY

READ 

Evidence for Water Antibonding Orbital Mixing in the Hydrated Electron from Its Oxygen 1s X-ray Absorption Spectrum

Xingpin Li, William J. Glover, et al.

OCTOBER 17, 2022

JOURNAL OF THE AMERICAN CHEMICAL SOCIETY

READ 

Get More Suggestions >